Available online at www.sciencedirect.com
SCIENCE DIRECT
Tectonophysics 421 (2006) 331–346
TECTONOPHYSICS
www.elsevier.com/locate/tecto

Crystallographic orientations of high-angle grain boundaries in dynamically recrystallized quartz: First results

Boriana Kuntcheva [a,✠], Jörn H. Kruhl [a,*], Karsten Kunze [b]

[a] Tectonics and Material Fabrics Section, Technische Universität München, D-80290 München, Germany
[b] Geologisches Institut, ETH Zürich, CH-8092 Zürich, Switzerland

Received 14 June 2004; received in revised form 1 April 2006; accepted 10 May 2006
Available online 30 June 2006

Abstract

The crystallography and geometry of high-angle grain boundaries from dynamically recrystallized quartz have been studied. On the basis of combined electron backscatter diffraction and universal stage measurements, the complete crystallographic orientation of the grain boundaries could be calculated. The u-stage rotation of the grain boundaries to a vertical position reveals that they are never curved but always consist of straight segments. Our results show that these segments preferentially occupy rhombohedral, trapezohedral and bipyramidal orientations, i.e., orientations in a ~25–50° girdle to the *c*-axis. A specific, albeit low, number of segments with special crystallographic orientation, with respect to a neighbouring quartz grain, often shows another special orientation with respect to the other neighbouring grain. Preferred combinations of grain boundary orientations related to both neighbouring grains are (i) low-index rhombohedral and high index trapezohedral, (ii) low-index bipyramidal and low-index trapezohedral or high-index rhombohedral, and (iii) low-index trapezohedral and low or high index trapezohedral. In certain cases, such as at triple junctions, the boundaries occupy specific trapezohedral orientations with a constant angle to the *c*-axis. This argues for energy isotropy of trapezohedral planes with the same angle to the quartz *c*-axis. In general, good match coincidence site lattice (CSL) orientations are not preferentially occupied so that most of the studied grain boundaries represent general boundaries. The formation of straight segments in special crystallographic orientations indicates the crystallographic control and implies an energy reduction of certain general boundaries.

Keywords: Coincidence site lattice (CSL); Crystallographic orientation; Electron backscatter diffraction (EBSD); Grain boundary migration; High-angle grain boundary; Quartz; Universal stage

1. Introduction

Grain and phase boundaries affect the petrophysical and rheological properties of rocks, such as strength, fluid permeability, susceptibility to weathering, resistance to cracking and corrosion (Mainprice et al., 1993; Aust et al., 1994; Shimada et al., 2002; Frary and Schuh, 2005, and references therein) and provide information about their tectonometamorphic history (Vernon, 2004). Vice versa, technical procedures have been applied to metals in order to tailor the character of grain boundaries and, consequently, improve the material properties (grain boundary engineering – Randle, 1997; Randle et al., 1999; Watanabe and Tsurekawa, 2004). Grain boundaries in metamorphic rocks, in particular, are formed and changed by recrystallization, defined as "nucleation

* Corresponding author. Tel.: +49 89 28925870; fax: +49 89 28925852.
E-mail addresses: kruhl@tum.de (J.H. Kruhl), kunze@erdw.ethz.ch (K. Kunze).
✠ Boriana Kuntcheva *8.10.1971–†9.11.2004

0040-1951/$ - see front matter © 2006 Elsevier B.V. All rights reserved.
doi:10.1016/j.tecto.2006.05.007

and migration of high-angle boundaries" (Vernon, 1976) or "deformation-induced reorganization of grain size, shape and/or orientation with little or no chemical change" (Poirier and Guillopé, 1979). During dynamic recrystallization and as a result of different lattice defect densities in neighbouring crystals, grain boundary

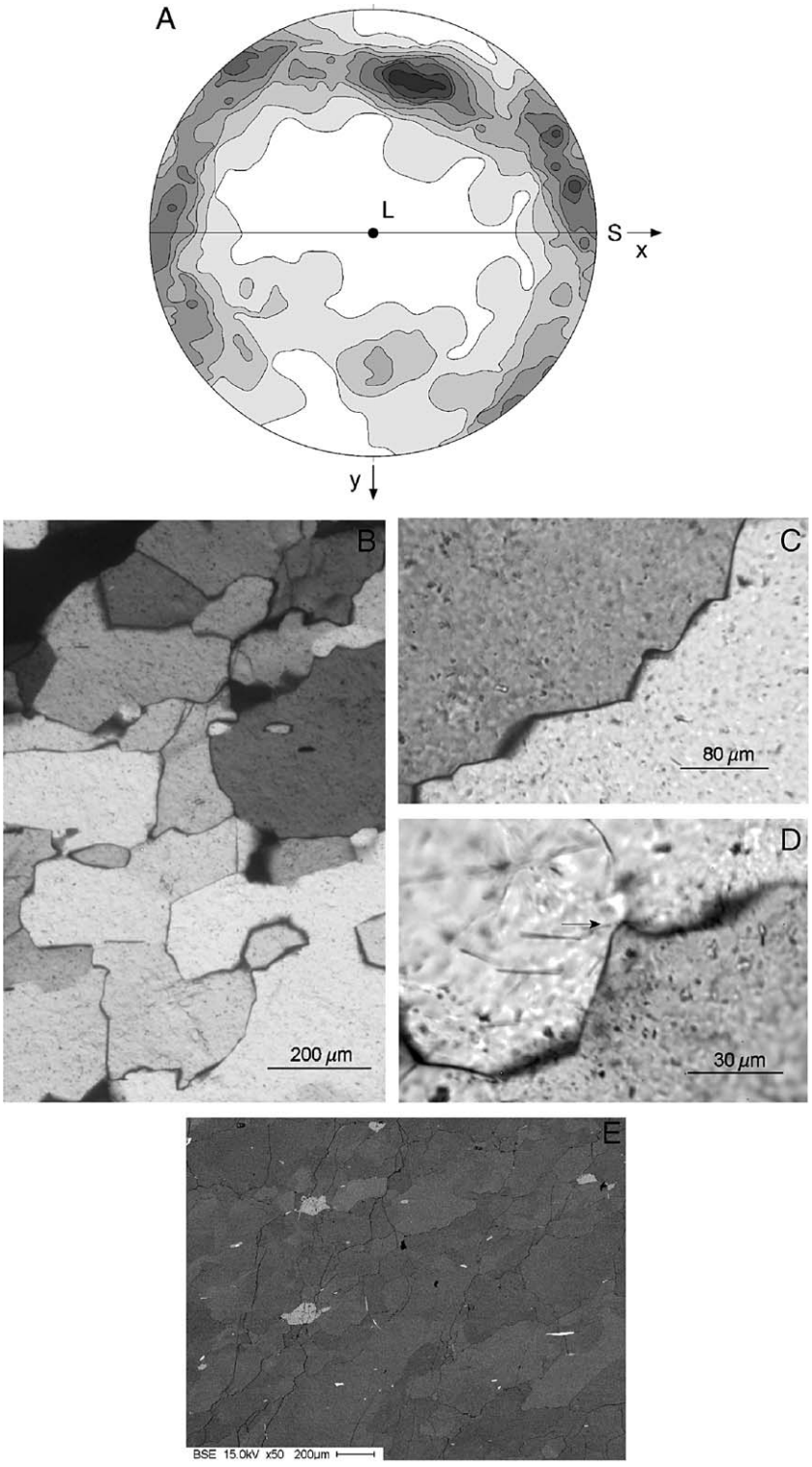

migration may lead to intense grain boundary suturing. The geometry of the sutured boundaries mainly depends on temperature, strain rate, finite strain and differential stress (Kruhl and Nega, 1996; Takahashi et al., 1998), but also on internal properties such as crystallographic orientations and the distribution and densities of lattice defects (Spry, 1969). During strain-induced grain boundary migration the length of the sutured quartz grain boundary segments increases with increasing temperature (Voll, 1969, p.117).

Quartz grain boundaries, formed during dynamic as well as static recrystallization, are rarely curved but consist of straight segments (Kruhl, 2001; Kruhl and Peternell, 2002). Voll (1960, 1969) points to a preferred crystallographic orientation of segments with mainly rhombohedral orientations at high temperatures. Based exclusively on universal-stage (henceforth u-stage) measurements of the angle between the quartz *c*-axis and the grain boundary pole, Kruhl and Peternell (2002) specified that the boundaries may occupy low- or high-index or even irrational orientations and, with increasing temperature, tend to be parallel to rhombohedral planes. However, the u-stage measurements of these investigations do not provide the full crystallographic orientation of quartz grain boundaries.

Our study, for the first time, presents the complete crystallographic orientation of quartz grain boundaries with respect to both neighbouring crystals and provides additional information on these crystallographic orientations with respect to specific grain boundary geometries, such as triple junctions or zigzag structures. Indications of crystallographic preferred grain boundary orientations are presented and possible reasons of grain boundary 'stability' are discussed. The results are based on a combination of electron backscatter diffraction (EBSD) measurements of crystal orientations and u-stage measurements of grain boundary orientations.

2. Theoretical background and current knowledge about the geometry of quartz grain boundaries

In general, grain boundaries represent a discontinuity in the lattice periodicity of neighbouring crystals and can be considered as a kind of planar defects (Read and Schockley, 1950; Hobbs et al., 1976; Bohm, 1995). With respect to the orientation of the rotation axis, which brings both neighbouring crystals in coincidence, two special types of grain boundaries are distinguished — tilt and twist boundaries (McLean, 1957; McLaren, 1986). If the rotation comprises tilt as well as twist components the boundary is referred to as general boundary.

Five macroscopic and three microscopic parameters (degrees of freedom) are required to completely describe the geometrical relationship along a general grain boundary (Read, 1953; Wolf, 1992). The three microscopic parameters are related to atomic-scale rigid-body translations parallel or perpendicular to the grain boundary plane, determined by relaxation processes, and are not subject of the present study. The five macroscopic degrees of freedom describe the orientation relationships and can be chosen in different ways.

a) The misorientation between two neighbouring crystals is a rotation of one crystal into the orientation of the other crystal. Therefore, it is completely described by three independent parameters, i.e., the misorientation angle and axis. The remaining two parameters are assigned to the grain boundary pole with respect to either crystal. Most of the previous studies on grain boundaries in rocks are based on the determination and interpretation of misorientations across grain boundaries (Fliervoet and White, 1995; Lloyd et al., 1997; Trimby et al., 1998). However, misorientation angles are not directly related to the crystallographic orientation of a grain boundary which determines the grain boundary properties and, therefore, misorientation angles cannot replace the crystallographic orientation data of grain boundaries.
b) The interface-plane scheme offers an alternative to choose the five macroscopic degrees of freedom. It assigns 4 parameters to the grain boundary pole with respect to both neighbouring crystals. The fifth independent parameter describes the angle of twist rotation about the grain boundary pole, while the tilt angle is determined by the grain boundary pole with respect to the two crystals (Wolf, 1992; Mainprice et al., 1993).

Fig. 1. (A) *c*-axis distribution of the studied paragneiss from the Sesia Zone, Val Loana, Western Alps; sample KR1231; 300 measurements. The u-stage reference frame is oriented with *X* parallel (E–W) and *Y* perpendicular to the foliation (N–S), and *Z* down-dipping parallel to the lineation. Solid lines = foliation; solid circle L in the centre = lineation; equal-area projection, lower hemisphere; contour intervals = 1 [m.u.d.], starting at 1. (B–D) Microstructures of the studied quartz grains; thin section photomicrographs; crossed polarizers; section perpendicular to the lineation and foliation; (B) part of the measured sample area with sutured and facetted grain boundaries, due to grain boundary migration during and after plastic deformation; (C) "zigzag" geometry of the measured quartz grain boundaries; (D) small grain-boundary peak (arrow) protruded over the more or less uniform boundary front. Since the photomicrograph is taken from a thin section inclined by 10° on the u-stage, only the central part is focused. (E) Orientation contrast image of part of the measured sample area, with partly poorly visible grain boundaries.

In particular, the latter approach has proven useful in recent HRTEM studies on metals and ceramics, which provide strong evidence of the importance of grain boundary orientations, such as atomic-scale faceting and frequent preference of asymmetrical rather than symmetrical boundary configurations (Wolf and Merkle, 1992, and references therein). In addition, recent studies on quartz indicate that grain boundaries with twin orientation relationships are only partly preferred (Kruhl and Peternell, 2002).

Our current knowledge about the geometry of quartz grain boundaries is restricted to certain twin boundary types, for which the existence of coincidence site lattice (CSL) models was geometrically and algebraically determined (McLaren, 1986; Grimmer and Kunze, 2004). However, according to McLaren (1986), the twin plane does not always coincide with the plane of densest CSL. Based exclusively on measurements of the angle between the quartz *c*-axis and the grain boundary pole, Kruhl and Peternell (2002) show that grain boundaries from dynamically recrystallized quartz do not preferentially occupy orientations parallel to good match twin planes.

Triple junctions are commonly described as linear defects where three crystals meet (King, 1999). It is assumed that at each triple junction (TJ) the balance of surface tensions and torque forces (function of the crystallographic orientations of grain boundaries) leads to local equilibrium (Herring, 1951). The equilibrium conditions affect the TJ geometry, defined by the three dihedral angles between the adjoining boundaries. If the grain boundary orientations are not crystallographically controlled, i.e., if the grain boundary energies are isotropic, for example, in monophase materials, the surface tension leads to the formation of dihedral angles of ~120° (Spry, 1969). According to Spry (1969), the grain boundaries at TJ can rotate or move and change from high-energy orientations, with respect to the neighbouring crystals, to lower energy orientations. The deviations of the dihedral angles from 120° reflect the effect of the anisotropic energy of the opposing grain boundaries (King, 1999). In addition, recent studies in material science have shown that, independently of the crystallographic orientations of the meeting boundaries, the TJ geometry is affected by the orientation of the triple line, i.e., the intersection line between the three boundaries (Adams et al., 1999; King, 1999; Gottstein et al., 2000). Based on a low-energy orientation of the triple line, a "pinning" or "friction" force, the "triple-line drag" (King, 1999), could arise and lead to a change of the dihedral angle at TJ.

3. Sample description and problem definition

The present study investigates quartz grain boundaries from garnet–biotite gneiss, a former kinzigite of the Sesia Zone (lower Val Loana, Western Alps, Italy). The gneiss was deformed and foliated during the first and second (D1 and D2) and refolded during the third Alpine deformation event (D3) at lower amphibolite facies temperatures, increasing to ~570 °C (Kruhl, 1979). During deformation quartz recrystallized and developed a crystallographic preferred orientation showing a cross-girdle distribution around the D2 lineation and slightly oblique to the foliation (Fig. 1A). The obliquity is interpreted as a result of D3 folding around the lineation.

The amphibolite facies conditions outlasted the deformation and, consequently, the quartz was annealed over a certain period during temperatures above the recrystallization temperature of quartz of ca. 300 °C

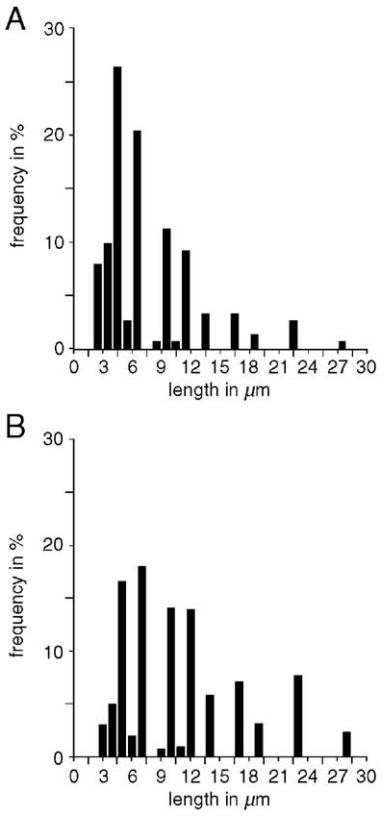

Fig. 2. (A) Frequency distribution of the length of 150 grain boundary segments from the measured thin section (Fig. 1). The segments form a continuous network, also including segments that are not used in other analyses for technical reasons as explained in the text. (B) Frequency distribution from A, but weighted by lengths of segments.

(Voll, 1976). This period is estimated as nearly 10 million years, based on cooling ages from the nearby Simplon–Antigorio region (Wagner et al., 1977). The quartz grains in the sample form up to 10 mm wide almost monomineralic layers with few isolated biotite and plagioclase grains (Fig. 1B). The quartz grains are 50 μm to 1 mm large and their axial ratios range from 1 to 2. The rare subgrains are mainly prism-parallel. The grain boundaries are strongly sutured and composed of straight segments, with lengths mostly between 2 and 30 μm (Fig. 2). But lengths of up to 100 μm can also occur. Locally, two sets of approximately parallel grain boundary segments may form "zigzag" structures (Fig. 1C). Locally, very long segments are interrupted by a short step, or small bulges protrude over an otherwise flat grain boundary front (Fig. 1D).

4. Methods

The complete crystallographic orientations of the grain boundaries were determined by a combination of u-stage and electron backscatter diffraction (EBSD) measurements. First, all grain boundaries, optically visible under crossed polarizers, with or without the gypsum plate, were manually digitized from the thin section using a drawing tube mounted on the polarizing microscope (Fig. 3). Since all grain boundaries are, to some extend, inclined to the thin section plane and, therefore, appear as more or less broad bands, only certain details of the grain boundary geometry are visible in plane view under the polarizing microscope. However, the u-stage allows the rotation of the inclined boundaries to a vertical position and, consequently, a more accurate registration of the grain boundary geometries. This technique represents a rather simple and fast method to determine the three-dimensional orientation of grain boundary segments and the geometry of grain boundary sutures on the micrometer-scale with sufficient accuracy.

4.1. Universal stage

The universal stage (u-stage; von Federow, 1893; Sarantschina, 1963) allows determining the spatial orientation of a straight grain boundary segment and of the quartz *c*-axis. The orientation of each boundary segment is recorded by the spherical coordinates of its pole relative to the thin section reference frame. Segments, down to the maximum resolution of the polarizing microscope of about 1–2 μm, can be

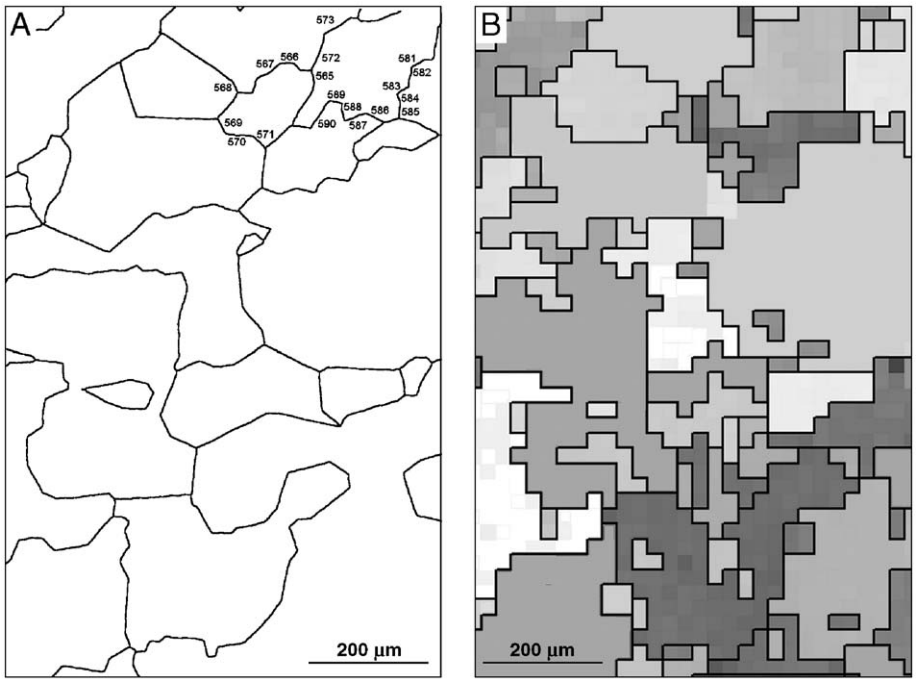

Fig. 3. (A) Thin section sketch of the same part of the measured quartz grain-boundary pattern shown in Fig. 1B. Each measured grain boundary segment is numbered as exemplified in the upper right part of the figure. (B) Orientation image map (OIM) of the same part of the measured thin section, as shown in A. The black lines represent grain boundaries between grains with misorientations > 15°. The rectangular grain boundary shape results from the step size of measurement (25 μm). The grey shades are related to different orientations of the crystals. Confidence index (CI) > 0.2.

measured. The measurement time is reduced by using a semi-automatic u-stage. The precision of the measurements, given by the inclination steps of the u-stage, approximates 0.5°. However, the error of measurement (estimated by repeated measurements) is ~ ±1° for the azimuth angle and ~ ±2° for the dip-angle. Due to three reasons, the u-stage cannot be applied for measurements of all grain boundaries in a thin section:

(1) The u-stage tilt is restricted to ca. 45° and, therefore, does not allow the rotation of flat grain boundary segments, i.e., with 0–45° dip with respect to the thin section plane, to a vertical position. Consequently, the orientation of these segments cannot be measured. This inability creates a bias in selecting the investigated boundary population and may change the probability of occurrence of certain crystallographic orientations. The statistical significance of this effect will be verified below.
(2) A zigzag geometry may lead to horizontal grain boundary stripes, with different inclinations, below the thin section surface. Consequently, they appear as diffuse grey bands and cannot be measured with sufficient accuracy.
(3) Grain boundaries inclined more than ~20° to the normal of the thin section plane appear more frequently diffuse when rotated to a vertical position because they are longer. Consequently, the measurement error is higher for these grain boundaries or most of them cannot be measured with sufficient accuracy.

4.2. Electron backscatter diffraction

The electron backscatter diffraction (EBSD) technique allows the local determination of the crystallographic orientation of a known crystal lattice (Venables and Harland, 1973; Adams et al., 1993). The EBSD system (EDAX-TSL OIM 3), equipped with a Digiview FW CCD camera, is installed on a SEM CamScan CS44LB at the Electron Microscopy Centre, ETH Zürich. Subsequently to mechanical grounding and in order to remove residual surface damage and to level any topography, the thin section was ultra-polished for 8 h, first with Al_2O_3 of 30-μm size and later with colloidal silica. For avoiding charging effects in the SEM the sample was coated by a few nm of carbon. A combined beam/stage scan was applied on measuring crystallographic orientations on a predefined surface area of 5000 μm × 1800 μm at a square raster of 25-μm steps. The data result in an orientation contrast image (Fig. 1E) and an orientation map which assigns a different colour to each 25-μm pixel, according to the measured crystal orientations (Fig. 3B). Due to weak EBSD pattern quality or different phases at some raster points, not all of the collected diffraction patterns were indexed with sufficient reliability. The indexing reliability is evaluated by a confidence index (CI) assigned to each measurement and ranging from 0 to 1 from low to high confidence, respectively. In the present study only measurements with CI > 0.2 were taken into account. The angular accuracy of the crystallographic orientation measured by EBSD is ~1° (Prior, 1999). The crystallographic orientations of the quartz grains, determined by the EBSD technique, are given as sets of Euler angles describing the specific rotations that transform the sample coordinate system into the crystal coordinate system and vice versa (Bunge, 1982).

4.3. Obtaining the crystallographic orientation of the quartz grain boundaries from the combination of u-stage and EBSD data

The practical determination of the crystallographic orientation of the grain boundaries on the basis of the u-stage and EBSD data is performed in two steps.

(1) The exact orientation of a digitized grain boundary segment is found on the EBSD orientation image map by graphical comparison with the grain boundary outlines sketched from the thin section. Usually, several data points of the EBSD measurement grid are covered by one quartz grain. Their orientations may vary as a result of lattice bending, subgrains and twins, but also as a result of measurement noise. From these data points an appropriate crystal orientation is selected, based on grid points with CI > 0.2 and as close as possible to the boundary segment without any subgrain boundaries in between. This is also checked by polarizing microscopy. Thus, for each u-stage orientation of a grain boundary pole (given in spherical coordinates) with respect to the thin section coordinate system, the EBSD crystallographic orientations (given in Euler angles) of both neighbouring grains are identified.
(2) The orientations of the grain boundary poles with respect to the crystal reference frame e of both neighbouring quartz grains are calculated by means of the rotation matrix derived from the Euler angles (Bunge, 1982), as shown by van Daalen et al. (1999, Appendix A). The rotation matrix represents the transformation of any direction

(here the grain boundary pole) from the sample into the crystal coordinate system. Based on the measurement errors of u-stage and EBSD data, the maximum combined inaccuracy was estimated ~3.5°.

The trigonal crystal symmetry of quartz leads to six equivalent crystal directions corresponding to the grain boundary pole. These six directions are represented by the one direction in the standard 120° sector on the upper hemisphere, spanned by two *a*-axes and the *c*-axis. This 120° sector consists of four 30° sub-sectors that carry equivalent hemimorphic (positive and negative) and enantiomorphic (right and left) forms, which are derived from the hexagonal holohedric (high symmetry) forms by discarding all mirror planes (Kleber et al., 1998, p. 86). For example, the four corresponding trapezohedral planes in the 120° sector are the left negative ($6\bar{1}5\bar{6}$), right positive ($51\bar{6}6$), right negative ($15\bar{6}6$), and left positive ($\bar{1}6\bar{5}6$) planes, all with the same angles to the *c*-axis and to the *a*-axes. Although these planes are not symmetrically equivalent, with respect to the quartz crystal structure, they are equivalent with respect to the hexagonal lattice (holohedry) spanned by the crystallographic axes of quartz. Therefore, they may show similar characteristics when constituting a grain boundary. For these reasons and the purpose of simplification, the grain boundary poles are also plotted in one fourth of the standard sector, i.e., in a 30° sub-sector on the upper hemisphere (equal area projection). In addition, density estimations are presented, based on the discrete data obtained by convolution with a Fisher distribution with a concentration parameter $k=30$, which were contoured in multiples of the uniform distribution [m.u.d.].

5. Results

5.1. Preferred crystallographic orientation of the measured quartz grain boundaries

The crystallographic orientations of all measured grain boundary segments are plotted in relation to the two neighbouring quartz crystals (Fig. 4). Each segment is represented by two crystallographic directions with respect to the crystal reference frames of the two neighbouring grains. The frequency distribution of the crystallographic orientations of the segments is non-uniform. Segments with angles of ~25–50° to the quartz *c*-axis dominate. They form a belt with several clearly separated maxima, mostly sub-parallel to some low-index rhombohedral and bipyramidal planes ($10\bar{1}1$, $30\bar{3}2$, $20\bar{2}3$, $11\bar{2}2$, $42\bar{2}1$) or to low-index trapezohedral planes ($41\bar{3}3$, $31\bar{2}3$, $51\bar{6}6$, $13\bar{4}4$, $13\bar{4}2$). However, maxima away from low-index planes do also occur and grain boundary segments sub-parallel to prismatic planes or to the basal plane are significantly less frequent.

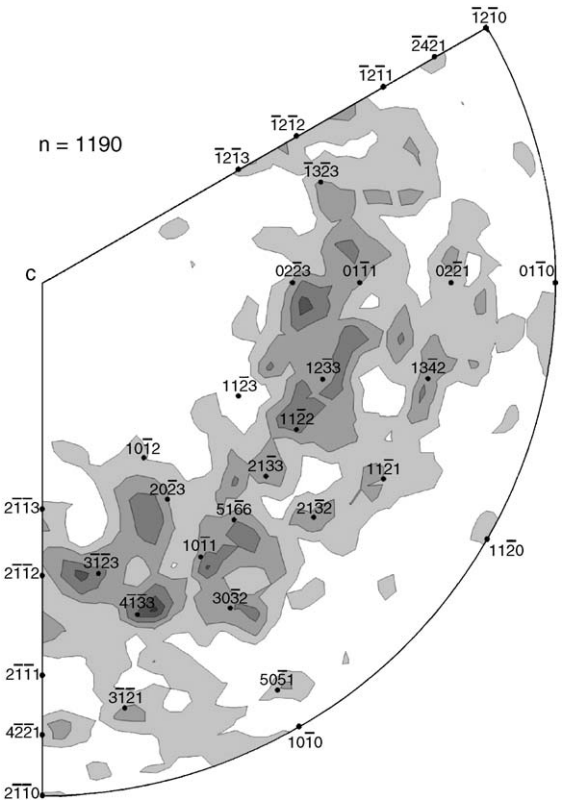

Fig. 4. Frequency distribution of all measured quartz grain boundaries (inverse pole figure, equal area projection, upper hemisphere). Each grain boundary is represented with respect to the crystallographic system of both neighbouring grains and, consequently, occurs in two different orientations. For comparison, low-index planes of quartz are indicated. Contour intervals=0.5 multiples uniform distribution [m.u.d.], starting at 1.

The frequency distribution of the data set, presented in Fig. 4 but reduced to the hexagonal holohedry and displayed in a 30° sector (Fig. 5), strongly underlines the preferred occurrence of grain boundaries with angles of ~25–50° to the *c*-axis. Within this narrow area of enhanced frequency, single maxima occur with up to 2.0 [m.u.d.] and 0.7 [m.u.d.] difference to the average density. These maxima are sub-parallel to the rhombohedral and bipyramidal planes (($10\bar{1}1$), ($20\bar{2}3$) and ($11\bar{2}2$)) or to certain low-index trapezohedral (($21\bar{3}3$) and ($51\bar{6}6$)) orientations.

Fig. 5 does not show the relationship between the two individual crystallographic orientations of any single grain boundary segment with respect to both neighbouring

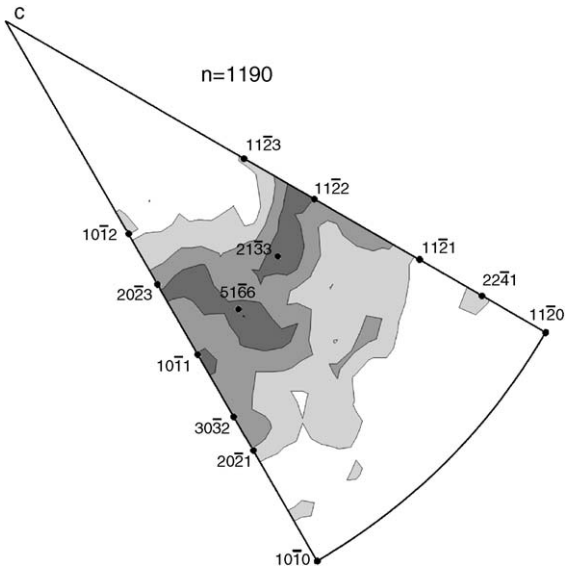

Fig. 5. Frequency distribution of all measured quartz grain boundaries shown in Fig. 4, but represented in a 30° segment of the quartz crystal system. Each grain boundary is shown in two orientations with respect to both neighbouring grains. Low-index planes are indicated. Inverse pole figure, equal area projection, upper hemisphere; contour intervals=0.3 [m.u.d.] starting at 1.

quartz crystals. The graphical representation of the relationship between these two orientations requires the simultaneous presentation of four parameters and an attempt for an appropriate representation is made as follows. Segments, forming specific maxima in Fig. 5 with one of their two orientations, are selected and their second position, with respect to the other neighbouring grain, is displayed separately (Fig. 6). The extension of each of the maxima is defined by the 1.6 [m.u.d.] contour since this density value represents the concentration threshold separating the maxima from the background, i.e., the general density of the belt distribution.

Fig. 6A indicates that grain boundary segments with rhombohedral (10$\bar{1}$1) orientations, with respect to one neighbouring grain, do not prefer low-index orientations with respect to the other grain. Their second position is parallel to high-index trapezohedral planes. In contrast, grain boundaries parallel to (11$\bar{2}$2), i.e., the Japanese twin plane, are preferentially related to the low-index trapezohedral plane (21$\bar{3}$3) or to certain prismatic planes (Fig. 6B). Single measurements also occur close to high-index rhombohedral or trapezohedral orientations. However, symmetrical orientations with the same (11$\bar{2}$2) orientation of both grain boundaries are not apparent.

Grain boundaries parallel to (20$\bar{2}$3), with respect to one neighbouring grain, prefer the trapezohedral orientations with an angle of 35–45° to the *c*-axis, with respect to the other grain. However, a few subprismatic grain boundary segments form a diffuse belt, 5–15° away from the prism orientations (Fig. 6C). The (21$\bar{3}$3) segments tend to have counterparts parallel to mainly trapezohedral orientations with angles of 25–50° to the *c*-axis (Fig. 6D). Within this area, single maxima close to relatively low-index trapezohedral planes ((32$\bar{5}$3), (32$\bar{5}$5), (31$\bar{4}$3)) occur, in addition to symmetrical (21$\bar{3}$3) orientations. The grain boundaries parallel to (5166), with respect to one neighbouring grain, do not show preferred low-index orientations with respect to the other grain (Fig. 6E). Nevertheless, they are not randomly distributed. Their orientation distribution forms maxima parallel to high-index trapezohedral orientations.

A similar representation for all measured rhombohedral and bipyramidal grain boundaries is made as follows. If a grain boundary is oriented sub-parallel (±3°) to any rhombohedral or bipyramidal plane, with respect to the one neighbouring grain, its orientation with respect to the other grain is represented (Fig. 7A, B). As for the (10$\bar{1}$1) boundaries (Fig. 6A), boundaries with two rhombohedral orientations are not preferred whereas the most favourable second positions are the high-index bipyramidal planes between (11$\bar{2}$2) and (11$\bar{2}$3). They form the strongest maxima with densities>3.5 [m.u.d.] (Fig. 7A). All other measurements in Fig. 7A do not show significantly preferred orientations within the range of the high-index trapezohedral planes. In contrast, the bipyramidal grain boundaries are clearly non-randomly distributed (Fig. 7B), with strongest concentrations near to (21$\bar{3}$3). Concentrations occur also close to the rhombohedral (10$\bar{1}$1) and (20$\bar{2}$3) planes as well as to the rhombohedral (11$\bar{2}$1) and trapezohedral (31$\bar{4}$2) planes.

In general, based on Figs. 6 and 7, it may be concluded that grain boundaries with a preferred low-index orientation, with respect to one neighbouring quartz grain, often also show a preferred orientation with respect to the other neighbouring grain. However, the second position is not always a low-index orientation. Combinations of two low-index orientations are apparent but not preferred. Moreover, at least one of the low-index orientations is a trapezohedral one. Frequent combinations of one low-index and one high-index orientation occur only if the low-index orientation is parallel to the rhombohedral plane (10$\bar{1}$1). High-index rhombohedral orientations, with respect to one neighbour, tend to be oriented parallel to bipyramidal planes, with angles of 40–50° to the *c*-axis, with respect to the other neighbour. The

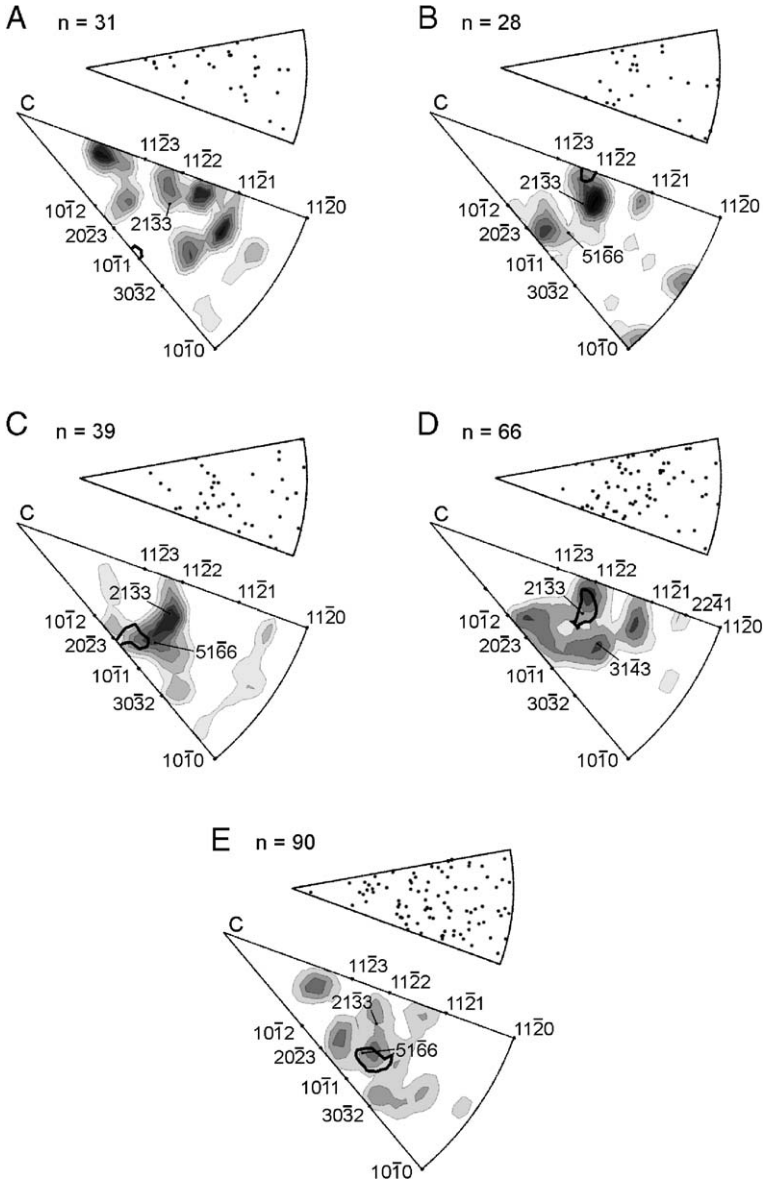

Fig. 6. Frequency orientation distribution of grain boundaries selected in relation to concentration maxima from Fig. 5. Each grain boundary is represented by two orientations with respect to either neighbouring crystal. If one of these grain boundary orientations belongs to a frequency maximum, represented by the bold lines in A–E, the second position is selected and presented in the frequency distribution diagrams; contour and pole representations; inverse pole figures; equal area projection, upper hemisphere; contour intervals = 0.5 [m.u.d.] starting at 1. (A) Orientations of grain boundaries with second position approximately parallel to (10$\bar{1}$1); (B) (11$\bar{2}$2); C. (20$\bar{2}$3); (D) (21$\bar{3}$3); (E) (51$\bar{6}$6).

bipyramidal planes prefer mainly the low-index trapezohedral (21$\bar{3}$3) planes but also the rhombohedral (10$\bar{1}$1) and (20$\bar{2}$3) planes.

5.2. Effects of statistical bias in the data sets

The preferred grain boundary orientations (Figs. 4–7) may be effected by crystallographic preferred orientations of the quartz grains with respect to the sample (thin section) reference frame. They may be additionally biased by the inability to measure all grain boundary inclinations by u-stage. Fig. 8 shows the distributions of *c*- and *a*-axes derived from crystal orientations, measured by EBSD, and of the grain boundary poles, measured by u-stage. Diagrams 8A and 8B show crystallographic preferred orientations of the measured quartz grains. The concentration of the grain boundary poles along the margin of the equal area

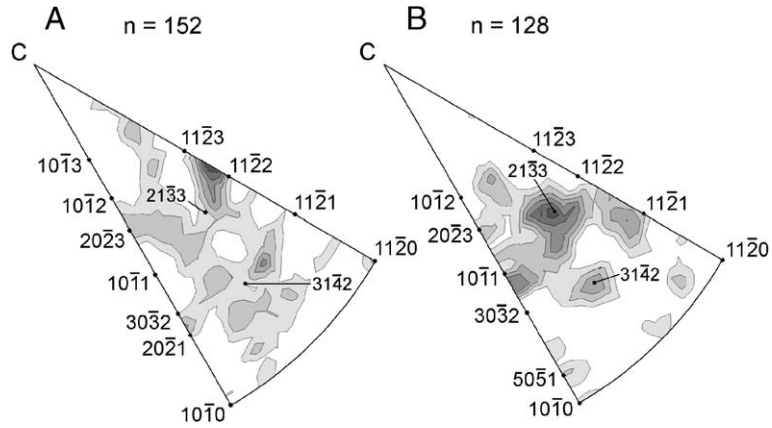

Fig. 7. Presentation analogue Fig. 6. (A) Orientations of grain boundaries with second position approximately parallel to any rhombohedral plane. (B) Second position approximately parallel to any bipyramidal plane. Inverse pole figure, equal area projection, upper hemisphere; contour intervals = 0.5 [m.u.d.] starting at 1.

projection (Fig. 8C) reflects the u-stage cut-effect plus a restricted measurability. The latter occurs due to the fact that the grain boundaries, inclined at low angles to the thin section plane, often appear diffuse under the microscope after their rotation to a vertical position. The effect of these non-random crystal and grain

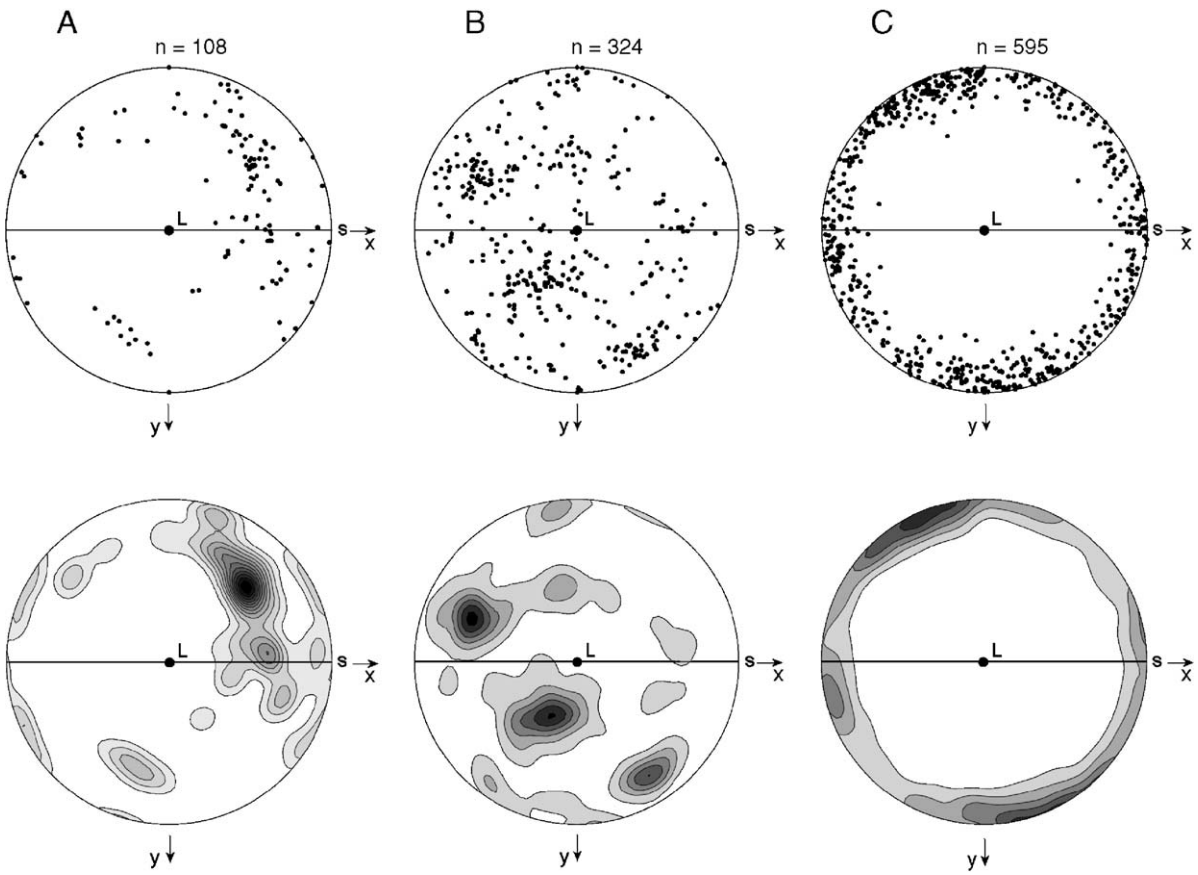

Fig. 8. (A) *c*-axis and (B) *a*-axes distribution of all measured quartz grains; (C) distribution of the measured grain boundary poles; pole (top) and contour (bottom) representations. The u-stage reference frame *X* and *Y* is shown; with *Z* down-dipping. Solid lines = foliation; solid circle L in the centre = lineation; equal-area projection, lower hemisphere; contour intervals = 1 [m.u.d.], starting at 1.

boundary orientation distributions on the preferred crystallographic orientations of the grain boundaries are evaluated as follows.

Sets of randomly distributed grain boundary poles (represented by spherical coordinates) and of randomly distributed crystal orientations (represented by Euler angles) are generated. On the basis of these sets, the orientations of 300 randomly distributed grain boundary poles, in the crystal system of 25 randomly distributed quartz grains, are calculated (Fig. 9A). In the same way, the crystallographic orientations of all measured grain boundaries, related to 25 randomly distributed quartz grains (Fig. 9B), as well as of 140 randomly distributed grain boundaries, related to all measured quartz grains (Fig. 9C), are determined. 3–5 additional calculations with different randomly distributed sets show similar results (not presented here). The random distribution of grains and their boundaries in the sample reference frame and the absence of crystallographic control lead to a random orientation of the grain boundaries in the crystal system of the grains (Fig. 9A). A similar distribution is observed if the orientations of random grain boundaries are represented in the crystal system of all measured grains (Fig. 9C). Thus, on the basis of Fig. 9C, it may be concluded that the non-random orientation of the measured quartz crystals does not significantly change the probability of occurrence of any crystallographic grain boundary orientation. On the other hand, the immeasurability of the strongly inclined grain boundaries slightly increases the probability of occurrence of prismatic grain boundaries by 1 to 1.5 [m.u.d.] (Fig. 9B). Thus, the absence of the u-stage constraints and measurements of all present grain boundaries might result in a slightly decreased (up to 1.5 [m.u.d.]) concentration of grain boundaries with 0–20° inclination to the *c*-axis and in a slightly increased concentration of all other boundaries in comparison to the data presented in Fig. 4. However, the effect of restricted measurability remains weak because most grain boundaries preferentially occur in a belt of ~25–50° to the *c*-axis.

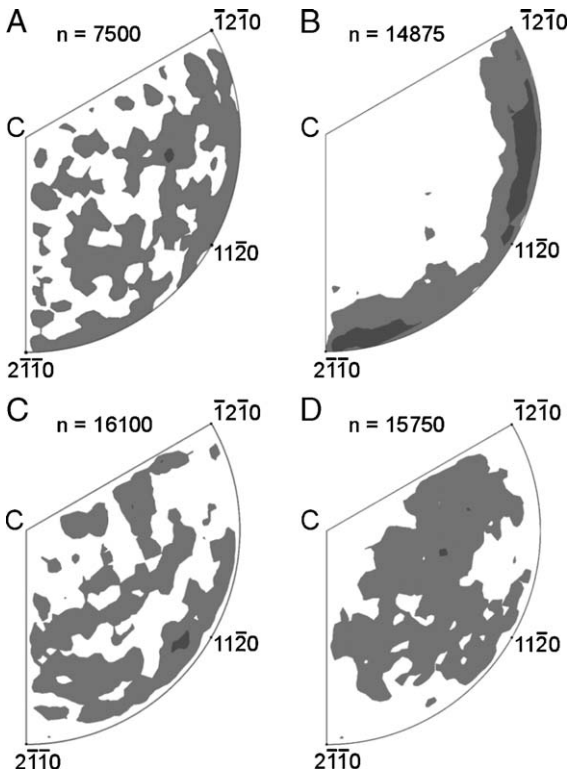

Fig. 9. Frequency distribution of grain boundaries represented in the crystallographic system of quartz. Inverse pole figures, equal-area projection, upper hemisphere; contour intervals = 0.5 [m.u.d.], starting at 1. (A) 25 randomly oriented quartz crystals, each related to 300 randomly oriented grain boundaries. (B) 25 randomly oriented quartz crystals, each related to all of the measured grain boundaries. (C) All measured quartz crystals, each related to 140 randomly oriented grain boundaries. (D) 350 grain boundaries and 45 quartz crystals, randomly chosen from all measured quartz crystals and grain boundaries.

As an additional test, 350 from all 595 measured grain boundaries are randomly selected and their crystallographic orientations calculated with respect to 45 quartz grains, randomly selected from all measured grains and without relationship to the selected boundaries (Fig. 9D). As for the randomly distributed grains and grain boundaries (Fig. 9A), the distribution of crystallographic orientations shown in Fig. 9D is almost random with a maximum density of 1.6 [m.u.d.]. Consequently, the crystallographic preferred orientations of the measured quartz grains and the restrictions of u-stage measurements do not significantly affect the observed pattern of crystallographic preferred orientations of the measured grain boundaries.

5.3. Crystallographic orientation of grain boundaries at triple junctions

Fig. 10A shows the crystallographic orientation of all measured grain boundaries at triple junctions, referred to the crystal system of both neighbouring quartz grains. The second crystallographic orientation of the grain boundaries which form distinct maxima with their first orientations are presented in Fig. 10B–E. The orientation distribution of the grain boundaries at triple junctions is non-random, with maxima of up to 3 [m.u.d.], the strongest ones near to the trapezohedral (2133), to the bipyramidal (11$\bar{2}$1), and to the mean rhombohedral (10$\bar{1}$1) plane. Compared to the frequency

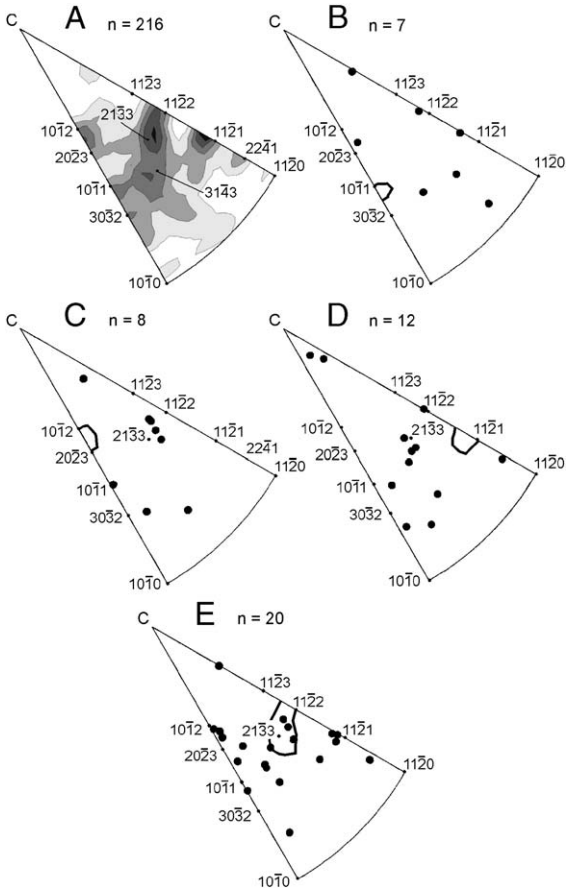

Fig. 10. (A) Frequency orientation distribution of all measured grain boundaries at triple junctions represented in the crystallographic system of both neighbouring grains. Presented are triple junctions with three as well as two or one measured grain boundaries. Inverse pole figures, equal-area projection, upper hemisphere; contour intervals=0.5 [m.u.d.] starting at 1. (B)–(E) Presentation similar to Fig. 6; bold lines encircle selected maxima from diagram A. (B) Orientations of grain boundaries with second position ~ ‖ (21$\bar{3}$3); (C) ~ ‖ (10$\bar{1}$2); (D) ~ ‖ (11$\bar{2}$1); E. ~ ‖ (10$\bar{1}$1).

distribution of all measured boundaries (Fig. 5), some similarities are evident, such as increased concentrations parallel to (21$\bar{3}$3) and (10$\bar{1}$1). As for all measured boundaries, only (21$\bar{3}$3) orientations occur as symmetric boundaries (Fig. 10B). Other preferred orientations, related to the second neighbouring grain of boundaries with their first orientations parallel to the (21$\bar{3}$3) plane, are the bipyramidal (11$\bar{2}$1), rhombohedral (10$\bar{1}$2) or high-index trapezohedral ones (Fig. 10C–E). Grain boundaries with the rhombohedral plane (10$\bar{1}$1) as first orientation have high-index bipyramidal and trapezohedral planes as second position (Fig. 10B). In general, the grain boundaries at triple junctions tend to be oriented in low-index rhombohedral or bipyramidal orientations with respect to one neighbouring quartz grain and in low- or high-index trapezohedral orientations with respect to the other quartz grain.

In order to determine the dihedral angles at triple junctions, the spatial orientations of all three grain boundaries at the TJ are required. In practice, the necessary u-stage measurements may not be realizable because of (i) the restricted inclination of the u-stage, (ii) the diffuse or irregular shape of buckled grain boundaries under the microscope, (iii) short and practically immeasurable segments directly at a TJ. During the present study full measurements on 12 triple junctions were performed. Except one, all of them show deviations of more than 10° from 120° for at least one of the dihedral angles, suggesting that the majority of the triple junctions in the measured sample contain angles different from 120°. Dihedral angles, including measurements from only two grain boundary segments at a TJ, vary from 90° to 164°, i.e., showing a similar range as silicate minerals in most metamorphic rocks (Vernon, 1968). These 'non-equilibrium' angles point to a strong anisotropy of grain boundary energies.

The crystallographic preferred orientations of the TJ boundaries with large (>130°) and small (<110°) dihedral angles clearly differ from each other (Fig. 11). Similar to the preferred orientation of all measured grain boundaries (Fig. 5), the TJ boundaries opposite to large angles concentrate in the "trapezohedral belt", with angles of ~25–50° to the *c*-axis. In contrast, the majority of TJ boundaries opposite to small angles avoid this "belt" and tend to be oriented closer and partly sub-parallel to the *c*-axis, i.e., sub-parallel to prismatic orientations such as (10$\bar{1}$1) and (11$\bar{2}$2).

Fig. 12 represents the crystallographic orientations of all measured triple lines in relation to the crystal system of the three neighbouring grains. The triple lines are

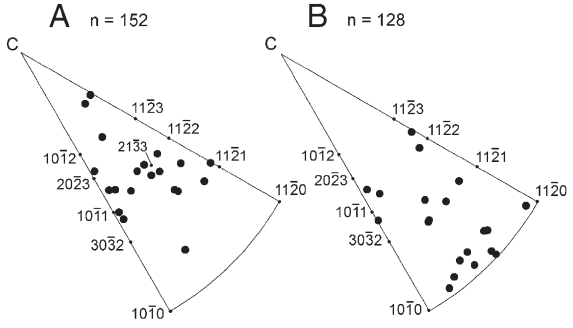

Fig. 11. Frequency distribution of grain boundary orientations at triple junctions opposite to dihedral angles of certain size; the grain boundaries are represented in the crystal system of both neighbouring quartz grains; inverse pole figures, equal-area projection, upper hemisphere. (A) Grain boundaries opposite to angles>130° (130–164°); (B) opposite to angles<110° (90–107°).

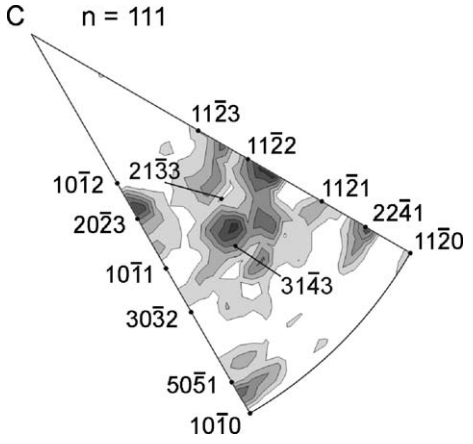

Fig. 12. Frequency distribution of the triple line orientations determined as intersection lines of the grain boundaries at triple junctions and presented in the crystal system of the three neighbouring quartz grains. Each triple line is represented by 3 positions. Included are triple lines based on only two measured intersecting grain boundaries. Inverse pole figure, equal area projection, upper hemisphere; contour intervals = 0.5 [m.u.d.], starting at 1.

preferentially oriented parallel to the pole direction of certain rhombohedral (20$\bar{2}$3 and 5051), bipyramidal (11$\bar{2}$2 and 22$\bar{4}$1) or high index trapezohedral planes. However, a larger data set is needed for a more detailed investigation.

6. Discussion

This study presents first results of investigations on sutured grain boundaries in dynamically recrystallized and post-tectonically annealed quartz and it contributes to the existing concepts of crystallographic orientations of quartz grain boundaries. Over a period of ca. 10 million years after decline of deformation the studied quartz experienced temperatures above the recrystallization temperature of ~300 °C, i.e., temperatures where grain boundary migration occurs. Within this period strain-induced grain boundary migration (Voll, 1960, p. 520; Spry, 1969) led to sutured grain boundaries. Since the development of sutured grain boundaries is a geologically short process, as discussed by Kruhl and Peternell (2002), it can be expected that the studied quartz grain boundaries reached their present positions already during the early stage of post-tectonic annealing. Consequently, it may be speculated that these positions did not change during continuous annealing and represent stable crystallographic orientations for the given geological conditions.

As shown for statically and dynamically recrystallized quartz (Kruhl, 2001; Kruhl and Peternell, 2002) as well as for metals and ceramics (Norton and Carter, 1992; Wolf and Merkle, 1992), the quartz grain boundaries from the present study also consist of straight segments and tend to facet. Although a curved boundary would reduce the surface area and thus decrease the free surface energy, compared to a facetted one, no curved boundaries are visible in the studied material on the micrometer scale, i.e., down to ca. 1–2 μm. Often zigzag structures of different size are formed. At the TJ, the dihedral angles generally deviate from 120°. All these observations on the geometry of the sutured grain boundaries indicate anisotropy of the grain boundary energies.

Our investigation shows that, as a result of amphibolite facies annealing after syntectonic recrystallization, segments of sutured quartz grain boundaries occupy crystallographic preferred orientations in a girdle of ~25–50° to the *c*-axis (Figs. 4 and 5). Within this girdle certain maxima of density distribution occur, however, no clear correlation to low-index planes is visible. This is valid for both orientations of the segments in relation to the neighbouring quartz grains. The comparison between the two orientations of a grain boundary segment to its two neighbouring grains reveals a more complex pattern of certain preferred combinations of orientations: (i) low-index rhombohedral and high-index trapezohedral, (ii) low-index bipyramidal and low-index trapezohedral or high-index rhombohedral, (iii) low-index trapezohedral and low or high index trapezohedral orientations (Fig. 6). In addition, certain differences in the favourable orientations between the rhombohedral and bipyramidal grain boundaries can be recognized. The rhombohedral boundaries, with respect to one adjoining grain, are often in high-index orientations with respect to the other grain and are almost never parallel to a second rhombohedral plane. In contrast, the grain boundaries with one bipyramidal orientation prefer certain bipyramidal or relatively low-index trapezohedral orientations with respect to the second neighbouring grain. In certain cases, such as at triple junctions, the boundaries "distinguish" between the "trapezohedral belts" with a constant angle to the *c*-axis, whereas within the belt these boundaries are distributed relatively randomly (Fig. 10). This fact argues, on one hand, for energy isotropy within the same "belt" of trapezohedral orientations with the same angle to the quartz *c*-axis, on the other hand, for energy anisotropy of orientations with different angles to the *c*-axis. However, all of these maxima comprise only a few measurements and the conclusions need to be confirmed by a larger data set.

In addition, at triple junctions with non-equilibrium dihedral angles, i.e., angles clearly deviating from 120°,

grain boundaries opposite to large angles preferentially show orientations within a 25–50° girdle to the quartz *c*-axis whereas grain boundaries opposite to small angles preferentially occupy orientations away from this girdle and partly sub-parallel to prismatic planes (Fig. 11). Since the relative energies of grain or phase boundaries at triple junctions are reciprocally proportional to the opposing angles (Smith, 1948; Vernon, 2004), it is inferred that quartz grain boundaries oriented with 25–50° to the *c*-axis have lower energies compared to grain boundaries sub-parallel to the *c*-axis. Consequently, the preferred orientation of all measured grain boundaries in the rhombohedral–trapezohedral belt (Figs. 4 and 5), but most of them not parallel to rhombohedral or trapezohedral planes, is interpreted as indication that grain boundaries preferentially occupy low-energy orientations as a result of post-tectonic annealing. However, it should be kept in mind that this interpretation is based on only 40 grain boundaries at triple junctions.

What is the relevance of these results with respect to the CSL theory which strongly influenced the grain boundary studies during the last decades, leading to the distinction between special boundaries of good fit and low energies (Spry, 1969; Bollmann, 1970; Pumphrey, 1976) and general boundaries without good atomic coherence and equally high grain-boundary energies? In general, the studied quartz grain boundaries do not show preferred low-index or CSL orientations with respect to both neighbouring grains, i.e., they do not represent special boundaries. Nevertheless, formation of facets and buckling of straight boundary segments indicate occupation of preferred crystallographic orientations and hence implies an energy reduction of certain general boundaries.

Our results are in agreement with recent studies on metals and ceramics which show that no simple relationship between CSL planes and grain-boundary energy exists (Wolf and Merkle, 1992; Saylor et al., 2003). Moreover, atom translations parallel to the grain boundary plane often disturb the existing CSL (Wolf and Merkle, 1992) indicating that other mechanisms for energy minimization are also involved. For quartz, McLaren (1986) concluded that for the most common twin types the twin composition plane is determined to some extend by the plane with the densest CSL. But the degree of matching across the boundary cannot always explain the formation of the twin boundaries and other factors may also exert influence. In addition, a large number of all boundary types exists, of which CSL boundaries represent only a small part. Saylor et al. (2003) distinguish between 6561 boundary types for MgO, of which less than 1% correspond to coherent CSL boundaries. This fact implies the statistical importance of general boundaries.

Finally, during the migration process, a grain boundary cannot be considered as isolated part of the texture that can freely "choose" the crystallographic orientation with lowest energy. The migration of the grain boundaries is affected by their geometrical positions within the grain boundary network and by the crystallographic orientation of the adjoining segments, so that the achievement of stable orientations may be constrained by lower mobility of neighbouring facets caused by their low-energy orientation. At triple junctions, a low energy orientation of one or two boundaries or of the triple line itself determines to some extend the orientation of the third adjoining boundary and, thus, suppresses the crystallographic control. Consequently, the number of geometrical and thermodynamic parameters affecting the formation of the grain boundaries leads to quite different grain boundary types, so that large data sets are required for a statistical investigation of grain boundary orientations.

7. Conclusions

Sutured quartz grain boundaries from a metamorphic rock, resulting from annealing after greenschist to mid-amphibolite facies deformation, were investigated by electron backscatter diffraction and universal-stage methods. For the first time, crystallographic preferred orientations of straight quartz grain boundary segments are presented. Measurements of totally 595 segments, in relation to both neighbouring quartz grains, provide results as follows.

1. The segments are preferentially oriented in a girdle of ~25–50° to the *c*-axis.
2. In detail, they occupy certain rhombohedral, trapezohedral and bipyramidal but mostly high-index or irrational orientations.
3. Grain boundaries with a preferred low-index orientation, with respect to one neighbouring quartz grain, often also show a specific preferred orientation with respect to the other neighbouring quartz grain. However, the second position is not always a low-index orientation and by far most pairs of orientations are both high-index or irrational.
4. In general, twin or other coincidence site lattice orientations are not preferred.
5. Quartz grain boundary segments with angles of ~25–50° to the *c*-axis have lower energies

compared to grain boundaries sub-parallel to the *c*-axis and the preferred occupation of such low-energy orientations is the result of post-tectonic annealing under mid-amphibolite facies conditions.

Acknowledgements

We wish to thank Renée Heilbronner and Geoffrey E. Lloyd for their detailed and careful reviews. This study was financially supported by the German Research Foundation (DFG) under grant KR691/30-1.

References

Adams, B.L., Wright, S.I., Kunze, K., 1993. Orientation imaging: the emergence of a new microscopy. Metallurgical Transactions 24A, 819–831.

Adams, B.L., Ta'asan, S., Kinderlehrer, D., Livshits, I., Mason, D.E., Wu, Chun-Te, Mullins, W.W., Rohrer, G.S., Rollett, A.D., Saylor, D.M., 1999. Extracting grain boundary and surface energy from measurements of triple junction geometry. Interface Science 7, 321–338.

Aust, K.T., Erb, U., Palumbo, G., 1994. Interface control for resistance to intergranular cracking. Materials Science and Engineering A 176, 329–334.

Bohm, J., 1995. Realstruktur von Kristallen. E. Schweizerbart, Stuttgart. 442 pp.

Bollmann, W., 1970. Crystal Defects and Crystalline Interfaces. Springer, Berlin/Heidelberg. 254 pp.

Bunge, H.-J., 1982. Texture Analysis in Materials Science. Butterworths, London. 593 pp.

Fliervoet, T.F., White, S.H., 1995. Quartz deformation in a very fine grained quartzo-feldspathic mylonite: a lack of evidence for dominant grain boundary sliding deformation. Journal of Structural Geology 17, 1095–1109.

Frary, M., Schuh, C.A., 2005. Grain boundary networks: scaling laws, preferred cluster structure, and their implications for grain boundary engineering. Acta Materialia 53, 4323–4335.

Gottstein, G., King, A.H., Shvindlerman, L.S., 2000. The effect of triple-junction drag on grain growth. Acta Materialia 48, 397–403.

Grimmer, H., Kunze, K., 2004. Twinning by reticular pseudomerohedry in trigonal, tetragonal and hexagonal crystals. Acta Crystallographica, A 60, 220–232.

Herring, C., 1951. Surface tension as a motivation for sintering. In: Kingston, W.E. (Ed.), The Physics of Powder Metallurgy. InMcGraw-Hill, New York, pp. 143–179.

Hobbs, B.E., Means, W.D., Williams, P.F., 1976. An Outline of Structural Geology. John Wiley & Sons, New York. 571 pp.

King, A.H., 1999. The geometric and thermodynamic properties of grain boundary junctions. Interface Science 7, 251–271.

Kleber, W., Bautsch, H.-J., Bohm, J., 1998. Einführung in die Kristallographie. Verlag Technik, Berlin. 416 pp.

Kruhl, J.H., 1979. Deformation and metamorphism of the southwestern Finero Complex (Ivrea Zone, N. Italy) and the northerly adjacent gneiss zone. Ph.D. Thesis, University of Bonn (in German).

Kruhl, J.H., 2001. Crystallographic control on the development of foam textures in quartz, plagioclase and analogue material. International Journal of Earth Sciences (Geologische Rundschau) 90, 104–117.

Kruhl, J.H., Nega, M., 1996. The fractal shape of sutured quartz grain boundaries: application as a geothermometer. Geologische Rundschau 85, 38–43.

Kruhl, J.H., Peternell, M., 2002. The equilibration of high-angle grain boundaries in dynamically recrystallized quartz: the effect of crystallography and temperature. Journal of Structural Geology 24, 1125–1137.

Lloyd, G.E., Farmer, A.B., Mainprice, D., 1997. Misorientation analysis and the formation and orientation of subgrain and grain boundaries. Tectonophysics 279, 55–78.

Mainprice, D., Lloyd, G.E., Casey, M., 1993. Individual orientation measurements in quartz polycrystals — advantages and limitations for texture and petrophysical property determinations. Journal of Structural Geology 15, 1169–1187.

McLaren, A.C., 1986. Some speculations on the nature of high-angle grain boundaries in quartz rocks. In: Hobbs, B.E., Heard, H.C. (Eds.), Mineral and Rock Deformation: Laboratory Studies — the Paterson Volume. In: Geophysical Monograph, vol. 36. American Geophysical Union, Washington, DC, pp. 233–245.

McLean, D., 1957. Grain Boundaries in Metals. Clarendon Press, Oxford. 346 pp.

Norton, M.G., Carter, C.B., 1992. Grain and interphase boundaries in ceramics and ceramic composites. In: Wolf, D., Yip, S. (Eds.), Materials Interfaces. Chapman & Hall, London, pp. 87–150.

Poirier, J.-P., Guillopé, M., 1979. Deformation-induced recrystallization of minerals. Bulletin de Minéralogie 102, 67–74.

Prior, D.J., 1999. Problems in determining misorientation axes, for small angular misorientations, using electron backscatter diffraction in the SEM. Journal of Microscopy 195, 217–225.

Pumphrey, P.H., 1976. Special high angle boundaries. In: Chadwick, G.A., Smith, D.A. (Eds.), Grain Boundary Structure and Properties. Academic Press, London, pp. 139–200.

Randle, V., 1997. The role of grain boundary plane in cubic polycrystals. Acta Materialia 46, 1459–1480.

Randle, V., Davies, P., Hulm, B., 1999. Grain boundary plane reorientation in copper. Philosophical Magazine 79A, 305–316.

Read, W.T., 1953. Dislocations in Crystals. McGraw Hill, New York. 228 pp.

Read, W.T., Schockley, W., 1950. Dislocation models of crystal grain boundaries. Physical Reviews. B 78, 275.

Sarantschina, G.M., 1963. Die Federow-Methode. VEB Deutscher Verlag der Wissenschaften, Berlin. 135 pp.

Saylor, D.M., Morawiec, A., Rohrer, G.S., 2003. Distribution of grain boundaries in magnesia as a function of five macroscopic parameters. Acta Materialia 51, 3675–3686.

Shimada, M., Kokawa, H., Wang, Z.J., Sato, Y.S., Karibe, I., 2002. Optimization of grain boundary character distribution for intergranular corrosion resistant 304 stainless steel by twin-induced grain boundary engineering. Acta Materialia 50, 2331–2341.

Smith, C.S., 1948. Grains, phases and interfaces: an interpretation of microstructure. Transactions of the American Institute of Mining, Metallurgical, and Petroleum Engineers Incorporated 175, 15–51.

Spry, A., 1969. Metamorphic Textures. Pergamon Press, Oxford. 350 pp.

Takahashi, M., Nagahama, H., Masuda, T., Fujimura, A., 1998. Fractal analysis of experimentally, dynamically recrystallized quartz grains and its possible application as a strain rate meter. Journal of Structural Geology 20, 969–975.

Trimby, P.W., Prior, D.J., Wheeler, J., 1998. Grain boundary hierarchy development in a quartz mylonite. Journal of Structural Geology 20, 917–935.

van Daalen, M., Heilbronner, R., Kunze, K., 1999. Orientation analysis of localized shear deformation in quartz fibres at the brittle–ductile transition. Tectonophysics 303, 83–107.

Venables, J.A., Harland, C.J., 1973. Electron backscatter patterns — a new technique for obtaining crystallographic information in the SEM. Philosophical Magazine 27, 1193–1200.

Vernon, R.H., 1968. Microstructures of high-grade metamorphic rocks at Broken Hill, Australia. Journal of Petrology 9, 1–22.

Vernon, R.H., 1976. Metamorphic Processes. Allen & Unwin, London. 247 pp.

Vernon, R.H., 2004. A Practical Guide to Rock Microstructure. Cambridge University Press, Cambridge/New York/Melbourne. 594 pp.

Voll, G., 1960. New work on petrofabrics. Liverpool and Manchester Geological Journal 2, 503–567.

Voll, G., 1969. Klastische Mineralien aus den Sedimentserien der Schottischen Highlands und ihr Schicksal bei aufsteigender Regional-und Kontaktmetamorphose. Habilitationsschrift, Fakultät für Bergbau und Hüttenwesen. Technische Universität Berlin, D83.

Voll, G., 1976. Recrystallization of quartz, biotite and feldspars from Erstfeld to the Leventina Nappe, Swiss Alps, and its geological significance. Schweizerische Mineralogische und Petrographische Mitteilungen 56, 641–647.

von Federow, E., 1893. Nouvelle méthode pour l'étude goniométrique et optique des cristaux appliquée à la minéralogie et à la pétrographie. Mémoir du Comité Géologique X (2), 1–191.

Wagner, G.A., Reimer, G.M., Jäger, E., 1977. Cooling ages derived by apatite fission-track, mica Rb–Sr and K–Ar dating: the uplift and cooling history of the central Alps. Memorie degli Istituti di Geologia e Mineralogia dell Università di Padova XXX, 1–27.

Watanabe, T., Tsurekawa, S., 2004. Toughening of brittle materials by grain boundary engineering. Materials Science and Engineering A 387–389, 447–455.

Wolf, D., 1992. Atomic-level geometry of crystalline interfaces. In: Wolf, D., Yip, S. (Eds.), Materials Interfaces. Chapman & Hall, London, pp. 1–57.

Wolf, D., Merkle, K.L., 1992. Correlation between the structure and energy of grain boundaries in metals. In: Wolf, D., Yip, S. (Eds.), Materials Interfaces. Chapman & Hall, London, pp. 87–150.